A Planar Array of Micro-Fabricated Electrospray Emitters for Thruster Applications

Luis Fernando Velásquez-García, Akintunde Ibitayo Akinwande, *Member, IEEE*, and Manuel Martínez–Sánchez

***Abstract*—This paper reports the design, fabrication, and experimental characterization of a planar array of micro-fabricated electrospray emitters intended for space propulsion applications in micro–satellites. The engine uses the ionic liquid EMI-BF_4 as propellant. Electrospray engines take advantage of the electrohydrodynamic effect known as Taylor cone to produce thrust. The array is designed with an open architecture and it is composed of a set of spikes, i.e., emitters, coming out from a propellant pool. There are two configurations for the emitters: fully sharpened slender emitters, i.e., pencils, and truncated pyramidal emitters, i.e., volcanoes. The arrays have between 4 and 1024 emitters in an active area of 0.64 cm^2. The surface of the engine (tank and emitters) is covered with "black silicon" that acts as wicking material. The micro-fabrication of the engine is described. The paper reports experimental characterization of the hydraulics system including wettability tests, current/emitter–voltage characteristics, and imprints of the exit stream on a collector. Preliminary results demonstrating the feasibility of obtaining substantially larger emission currents at the same extraction voltage by controlling the temperature are also reported. The paper compares the experimental current/emitter–voltage characteristics with relevant theories of field emission of electrons. [1433]**

***Index Terms*—Black silicon, electrospray emitter array, ionic liquid propellant, propulsion.**

I. Introduction

EMPIRICAL documentation on electrospray emission can be tracked back to the beginning of the seventeenth century [1]. Probably the first person to report the emission of charged particles from a conductive liquid meniscus in recent times was Zeleny [2]. It was not until many years after his work that Taylor proposed a simple model to explain the conical shape of a meniscus under the influence of an electric stress larger than a critical value; this explanation describes to first-order what has since been known as the Taylor cone effect [3].

Within a few years after the publication of the work of Taylor, papers on colloid thruster technology appeared, in particular a series of papers authored by Perel and Mahoney [4]–[8]. Their work focused on pressure fed colloid thrusters that use low vapor pressure doped solvents and extraction voltages that make the engine work in the highly stressed, i.e., multiple Taylor cone, regime.

In 1975, Bailey published a paper on the temperature and capillarity effects for colloid thrusters, specifically in surface tension driven propellant flow [9]. Such work concluded that capillary-fed engines can perform as well as positive pressure-fed engines, even with wide temperature variations.

The renewed interest on electrospray thruster technology in the last years came mainly because of the appearance of new space applications that require scaled-down efficient space engines [10], and the advance in several fields during the 80's and early 90's, in particular spray ionization and micro-fabrication [11], that made feasible low-startup-voltage, batch uniform electrospray emitter arrays.

Recent work has been done on macro-sized colloid thrusters that operate in the single Taylor cone regime and use doped solvent as propellant, in particular by Hruby *et al.* [12]. Work on internally-fed, micro-fabricated colloid thruster arrays that work in the droplet emission single Taylor cone regime has also been carried out, in particular by Paine [13], [14], Xiong [15], [16], and Velásquez-García [17]–[19].

It has been known for some time that if the propellant is conductive enough, and the flow rate is small enough, the Taylor cone can emit solvated ions in a mixed regime [20]. The first report on stable Taylor cones using high conductive ionic liquids was made by Fuller *et al.* [21]. In the year 2003 it was demonstrated experimentally that it is possible to extract only ions from electrospray sources that use ionic liquids [22]–[24]. Ionic liquids are salts formed with relatively large organic cations and anions that remain liquid at or near room temperature. In particular, the ionic liquid EMI-BF_4 is composed of the cation ethyl-methyl-imidazolium (EMI^+) and the anion tetrafluoroborate (BF_4^-). EMI-BF_4 is ideal for space propulsion applications because of its physical and electrical properties, such as near zero vapor pressure and large electrical conductivity [22], [25]. The ionic liquid EMI-BF_4 is known to emit two species, in a rather fixed mix ratio; the emitted species are a monomer with a mass of 111 amu, and a dimer with a mass of 309 amu [23].

The thrust efficiency η_T is defined as the ratio between the beam usable power and the supplied power. For the case of a beam composed of two monochromatic charged species η_T is given by [26]

$$\eta_T = \eta_i \cdot \eta_{tr}^2 \cdot \eta_\theta \cdot \eta_E \cdot \eta_p \tag{1}$$

where η_i is the ionization efficiency, η_{tr} is the transmission efficiency, η_θ is the angular efficiency, η_E is the energy efficiency,

Manuscript received September 4, 2004; revised November 15, 2005. this work was supported by the Air Force Office of Scientific Research (AFOSR) under Grant F49620-01-1-0398, managed by Dr. M. Birkan. Subject Editor Y.-C. Tai.

L. F. Velásquez-García is with the Department of Aeronautics and Astronautics and Department of Electrical Engineering and Computer Science, Massachusetts Institute of Technology, Cambridge, MA 02139 USA (e-mail: lfvelasq@mit.edu).

A. I. Akinwande is with the Department of Electrical Engineering and Computer Science, Massachusetts Institute of Technology, Cambridge, MA 02139 USA (e-mail: akinwand@mtl.mit.edu).

M. Martínez–Sánchez is with the Department of Aeronautics and Astronautics, Massachusetts Institute of Technology, Cambridge, MA 02139 USA (e-mail: mmart@mit.edu).

Digital Object Identifier 10.1109/JMEMS.2006.879710

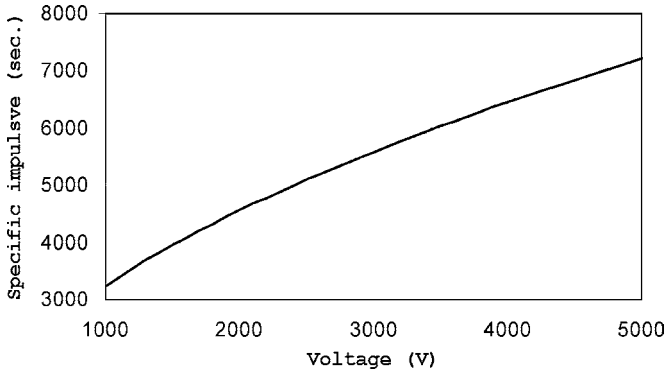

Fig. 1. Specific impulse $I_{\rm sp}$ versus tested voltage for an electrospray thruster that uses EMI-BF_4 as propellant. The substantially larger $I_{\rm sp}$ that can be obtained by using EMI-BF_4, compared to electrospray thrusters that emit droplets, translates in larger mass savings and therefore, the engine would fare better in long-term missions.

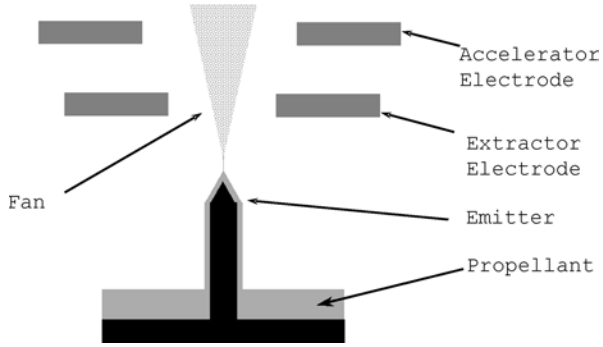

Fig. 2. Schematic of an externally fed electrospray emitter. The propellant is moved by the wicking material covering the hydraulics, due to surface tension effects. The extractor electrode creates an ion-emitting Taylor cone on each emitter. The accelerator gives to the stream the desired velocity, which determines the specific impulse.

and η_p is the propulsive efficiency related to polydispersity. The ionization efficiency is to first order 1 because the ionic liquid EMI-BF_4 has a very small vapor pressure (so far undetermined), thus only ionized species make up the beam. The transmission efficiency is larger than 99% because the angular spread of the beam is relatively low and well contained, and it is assumed a good optical design to keep low the ion interception with the electrodes. The angular efficiency is estimated to be better than 98% for the beam divergence that has been measured on EMI-BF_4 sources [26], [27]. The propulsive efficiency associated with polydispersity, is

$$\eta_p = \frac{\left[1-\left[1-\sqrt{\delta^*}\right]\cdot\beta\right]^2}{\left[1-\left[1-\delta^*\right]\cdot\beta\right]} \tag{2}$$

where δ^* is the heavier particle to lighter particle specific charge ratio (equal to 0.36 for the case of EMI–BF_4), and β is the fraction of the total current carried by the lighter particle, is set at 95.5%. The energy efficiency is defined as the ratio $\Delta V/V$ of extraction voltage drop to total voltage. For low currents ΔV is no more than a few volts [26]. The energy difference is probably invested in extracting charged species directly from the liquid surface. In conclusion, an electrospray engine that uses the ionic liquid EMI-BF_4 should have an overall propulsive efficiency in the 86% to 91% range [26]. The excellent propulsive efficiency of an electrospray engine using the ionic liquid EMI-BF_4 as propellant is accompanied by large specific impulse values, as seen in Fig. 1. The specific impulse $I_{\rm sp}$ is defined as

$$I_{\rm sp} = \frac{F}{\dot{m}\cdot g} \cong \frac{c}{g} \tag{3}$$

where F is the thrust, $\dot{m}$ is the mass flowrate, g is the gravity's constant and c is the exit stream velocity. Therefore, it is possible to build efficient engines with a different specific impulse and thrust range compared to electrospray engines based on droplet emission. The ionic liquid EMI-BF_4 has a very low-vapor pressure, making it suitable to be used in an open architecture engine, as shown in Fig. 2. This architecture has been demonstrated for a single tungsten needle by Lozano *et al.* [27].

The emission of charged particles implies leaving on the counter-electrode reactive species that can produce electrochemical effects if a sufficient double-layer voltage is allowed to build up. Recent preliminary work has demonstrated that ac operation of bipolar electrospray sources using ionic liquids solves both the problem of the engine charge neutrality and the electrochemical effects, making the concept of using ionic liquids in electrospray engines feasible [28].

This paper proposes an electrospray engine that operates in the single Taylor cone regime emitting solvated ions. The engine utilizes an open architecture and the ionic liquid EMI-BF_4 as propellant. The engine, illustrated in Fig. 2, is surface tension driven. It is important to mention that externally fed electrospray engines are not a true novelty because field emission electric propulsion (FEEP) and liquid metal ion sources (LMISs) use this source architecture [29]. What is novel in this work is the extension of the use of an organic propellant by the introduction of a method to produce many small, uniform emitters made of silicon in a small area, including field enhancement features, and the corresponding surface treatment to achieve wettability.

The engine lacks static pressure difference between the plenum and the emitters; therefore, there cannot be propellant emission unless it is electrically activated. In this sense, the architecture of the planar array is less vulnerable to unplanned propellant emission compared to pressure fed schemes. In the proposed engine there is a flowrate match between the engine hydraulics and what a Taylor cone can emit in a steady form. The engine has a certain maximum pumping capability based on the interaction of surface tension pulling and viscous losses, and so the engine can deliver to the Taylor cones as much propellant as requested up to a certain maximum flowrate value. Clogging is not an issue in this engine because the propellant is not doped and the flow channels are open.

II. The Planar Array

Fig. 3 is a schematic of a proposed engine, structured with micro-fabricated electrodes. *Wafer 1* has the accelerator electrode features, *Wafer 2* has the extractor electrode features, and *Wafer 3* has the engine hydraulics. The electrodes are made of heavily doped polycrystalline silicon to make the device CMOS-compatible.

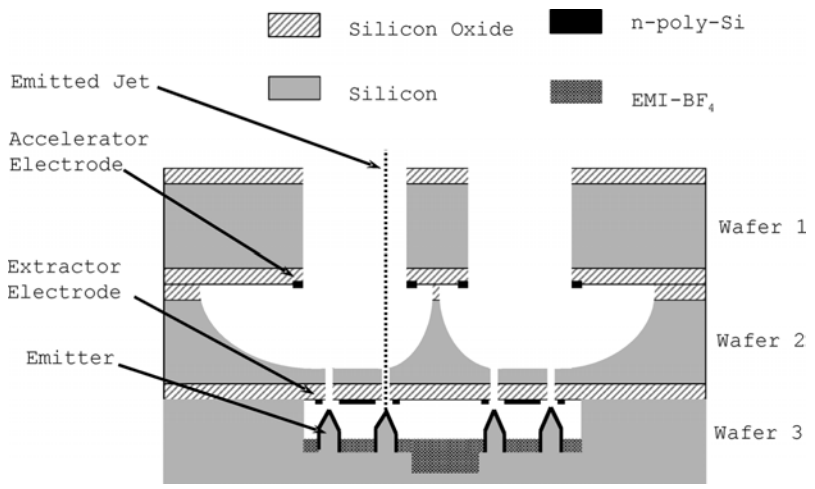

Fig. 3. Schematic of the proposed planar electrospray thruster array with micro-fabricated electrodes.

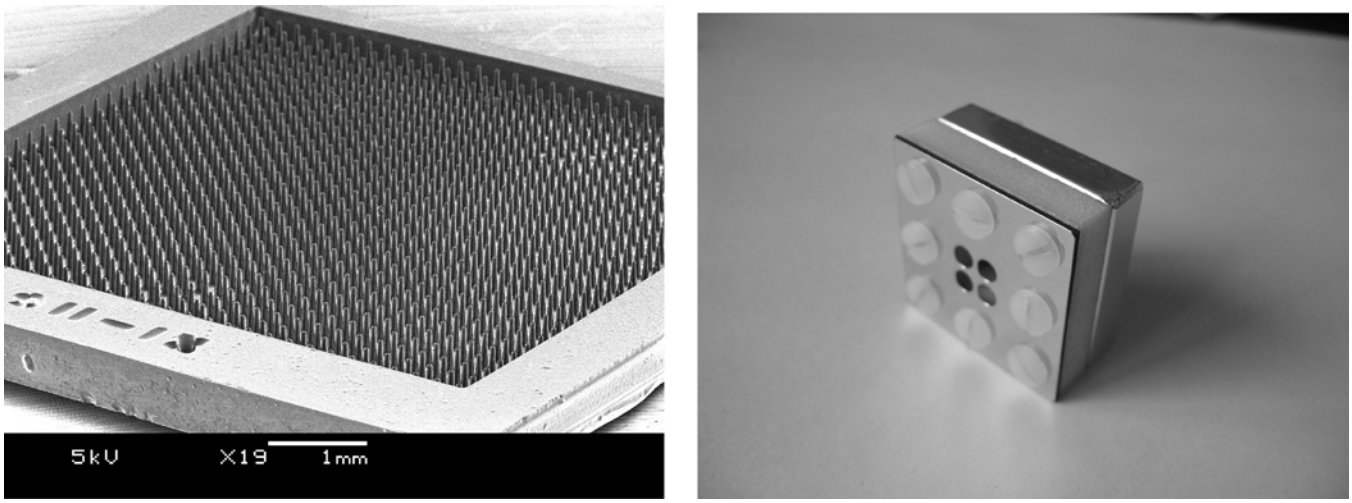

Fig. 4. A 32×32 pencil emitter array (left), macro-fabricated electrodes for a 2×2 volcano emitter array with its external extractor/package (right).

To obtain a proof-of-principle for the device, several hybrid test devices were fabricated and tested, where the electrodes where macro-fabricated and externally provided. The implemented planar arrays have one propellant pool containing between 4 and 1024 emitters in a 0.64 cm^2 area. Two types of emitters were implemented: fully sharpened slender emitters, called *pencils*, and truncated pyramidal emitters, called *volcanoes*. The two types of emitters respond to different trade-offs between emitter performance and fabrication robustness [18]. Fig. 4 shows an emitter array composed of 1024 pencil emitters, and the external electrodes for an emitter array composed of four volcano emitters; as a guideline, the emitter-to-emitter separation of the 32×32 pencil array is 200 μm. Fig. 5 illustrates the morphology of the two emitters implemented in the planar array. Volcano emitters are intended to emit from each of the sharp tips at the top surface boundary with a tilt close to 45° while pencils are expected to emit almost parallel to their axis. Typical dimensions for a volcano emitter are: $L_{c,o}$ (the diameter of the circle that circumscribes the flat top emitter surface) equal to 90 μm, L_c (radius of curvature of the top surface – to – lateral surface transition) equal to 6 μm, height equal to 270 μm; typical dimensions for a pencil emitter are: $L_{c,o}$ (the size of the pencil body) equal to 50 μm, L_c (radius of curvature of the emitter tip) equal to 3 μm, height 270 μm.

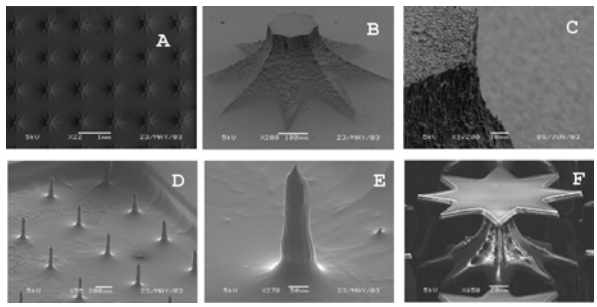

Fig. 5. Selected pictures of emitters implemented in the planar array. (A) Top view of a volcano forest; (B) single volcano; (C) volcano emitter tip; (D) pencil field; (E) single pencil; (F) pencil emitter midway in its fabrication process.

In operation, a thin propellant film covers the emitters of the engine. The shape of the propellant free surface is determined

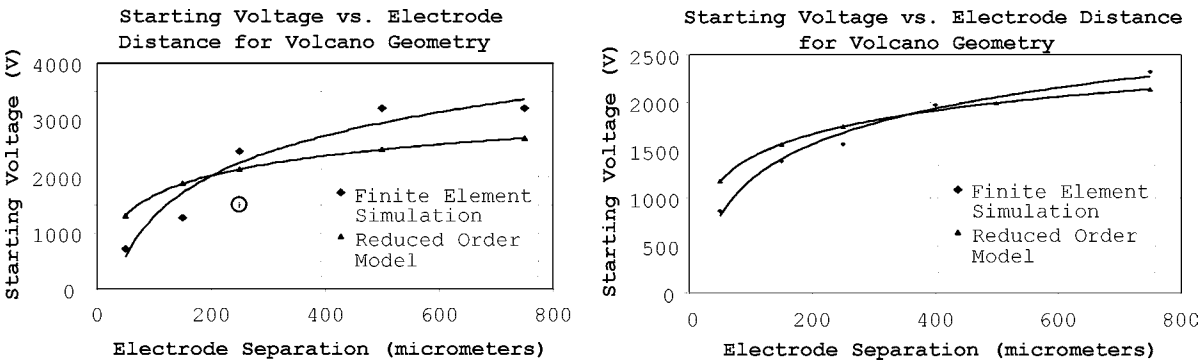

Fig. 6. Start-up voltage versus extractor separation for two volcano emitters using EMI-BF_4. The plot on the left models an emitter with the same geometry of the emitter modeled in the plot of the right, but with dimensions twice as large. The experimental points (coming from the testing facility with a fixed emitter-to-electrode separation equal to 250 μm) fall inside the circle drawn on the left plot, about 25% off from the theoretical estimates. There is good agreement between the finite element simulations and the reduced-order model; there is also corroboration of the modeling from the experimental data.

by the interaction between the emitter shape, surface tension effects, and electrostatic pulling. When the electric field is larger than a certain threshold, the surface tension effects cannot any longer counteract the electrostatic pulling. The normal electric field E_n acting on the free surface near an emitter sharp tip is given by [30]

$$E_n = \psi \cdot \frac{V}{\sqrt{L_{c,o} \cdot L_c}} \tag{4}$$

where V is the applied voltage, L_c is the radius of curvature of the sharp tips, $L_{c,o}$ is the diameter of the emitter head, and ψ is a dimensionless factor. Therefore, the threshold electric field $E_{n,\mathrm{start}}$ obeys the following relationship:

$$\frac{\varepsilon_o}{2} \cdot E_{n,\mathrm{start}}^2 > \lambda \cdot \frac{\gamma}{L_c} \tag{5}$$

where ε_o is the electrical permittivity of free space, γ is the surface tension of the liquid, and λ is a dimensionless factor. In order to explore the design space, we ran a series of finite element simulations of the electric field around the emitter tips using the commercial software Maxwell on the designed emitter geometry. The emitter-to-extractor separation was varied for the fixed geometry. Also, the designed emitter geometry was scaled-down to 50%, and a similar set of finite element simulations were carried out for a range of emitter-to-extractor separations. We found good agreement between the 3-D finite element simulations and the reduced order model that predicts the starting voltage V_{start} as [18]

$$V_{start} = \sqrt{\frac{\gamma \cdot L_{c,o}}{\varepsilon_o}} \ln\left[\frac{4G}{\sqrt{L_c \cdot L_{c,o}}}\right] \tag{6}$$

where G is the emitter-to-extractor separation, and $4G > (L_c.L_{c,o})^{0.5}$. Fig. 6 illustrates the agreement between finite element analysis and the reduced order model for the volcano emitter type, as well as the corroboration of the modeling by the experimental data.

Fig. 7 shows the estimated thrust of a 32×32 pencil array based on the specific charge from the literature [22] and the *I–V* characteristics (see Section IV) of an 8-tip volcano emitter array heated to a temperature of 51.3 °C, assuming even distribution

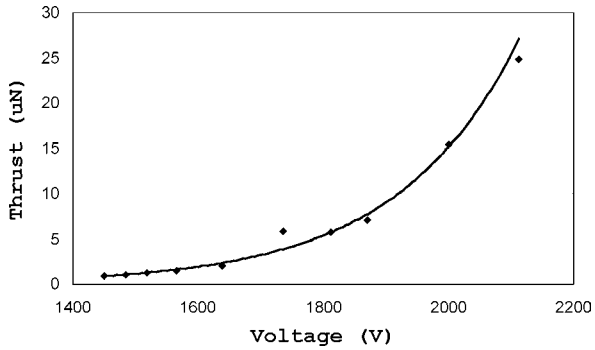

Fig. 7. Thrust versus voltage for a 32×32 pencil emitter array (0.64 cm^2 of active area) based on I_{sp} estimates and *I–V* characteristics of a heated volcano emitter planar array.

of the volcano emission from each of the sharp corners. The thrust was calculated using the following expression:

$$F = \dot{m} \cdot c = g \cdot I_{\mathrm{sp}} \cdot \frac{I}{\frac{q}{m}} \tag{7}$$

where q is the species charge, m is the species mass, and I is the emitted current. We estimate that one of these devices can deliver thrust in the 2–28 micro-Newton range, for voltages up to 2500 V. For the thrust range and the I_{sp} values that this device can achieve, we think that the engine would be ideal for any precisely controlled, low-thrust, time-nonlimited mission for micro-satellites, in particular deep space missions.

III. Micro-Fabrication of the Planar Array Hydraulics

The following is the fabrication process of the implemented planar array, corresponding to the fabrication of the engine hydraulics and field enhancement system. The emitter generation is achieved using a novel micro-fabrication process to obtain deep (> 250 μm) 3-D features using hanging etching masks with nonpassivated deep-reactive ion etching (DRIE). The fabrication of a fully micro-fabricated array, including a brief description of the corresponding set of optical masks, is discussed in the cited reference [18]. Fig. 8 shows a graphical summary of the process flow.

1) Deposition a thick layer of plasma-enhanced chemical vapor deposited (PECVD) silicon oxide on both sides of

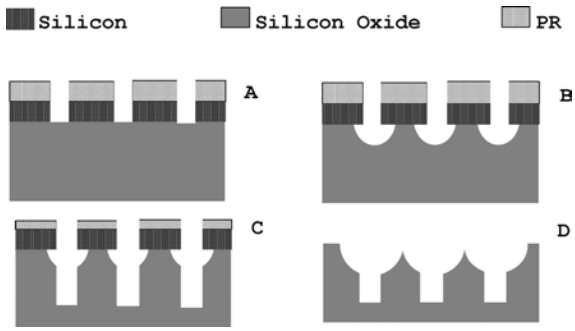

Fig. 8. Schematic to illustrate the emitter micro-fabrication process. (A) top silicon oxide layer patterning; (B) starting of emitter sharpening; (C) propellant pool and emitter height definition; (D) completion of emitter sharpening.

the substrate. The film thickness is set by the selectivity of the DRIE recipes that are used in the process flow.

2) Transfer of regions to form the propellant pools and the emitters to the silicon oxide film on the top surface of the substrate [see Fig. 8(a)].
3) Isotropic DRIE of silicon using SiO_2 as mask [see Fig. 8(b)].
4) Anisotropic DRIE of silicon using SiO_2 as mask [see Fig. 8(c)].
5) Complete emitter sharpening using isotropic DRIE. Remove the silicon oxide from both sides using 49% pure Hydrofluoric acid (HF) [see Fig. 8(d)].
6) Wicking material formation. Form *black silicon* [31] on the surfaces of the engine hydraulics.

IV. Experimental Results

Experimental characterization of the hydraulics system included wettability tests, current/emitter–voltage characteristics, and imprints of the exit stream on a collector. There are also included preliminary results demonstrating the feasibility obtaining substantially larger emission currents at the same extraction voltage by controlling the temperature.

A. Wettability Tests

The first series of tests carried out on the planar array was intended to qualitatively verify smooth propellant flow to the emitters, and diagnose the change in the wettability properties due to the *black silicon* treatment. As pointed out in the previous section, silicon cannot be properly wetted by EMI-BF_4 unless a *black silicon* treatment is performed on its surface. Several other surface treatments, such as thin film deposition of PECVD silicon oxide, physical vapor deposited (PVD) aluminum, and PECVD silicon nitride, were explored without success. It was experimentally determined that the optimum *black silicon* formation time, using a LAM 490B plasma etcher with the parameters listed in Table I, is around 10 min. Fig. 9 shows an Atomic Force Microscope picture of a silicon surface after 10 minutes of exposure to a *black silicon* surface treatment has been carried out. The picture was taken using an Autoprobe CP Atomic Force Microscope. The average surface roughness was found to be equal to 137.15 nm. The *black silicon* treatment creates on the surface an intricate network of trenches

TABLE I
Summary of the Parameters Used to Formation of Black Silicon Using a LAM 490B Plasma Etcher

PARAMETER	VALUE
Pressure (mTorr)	200
RF Power (W)	200
Gap (cm)	0.5
Helium (sccm)	30
Chlorine (sccm)	150

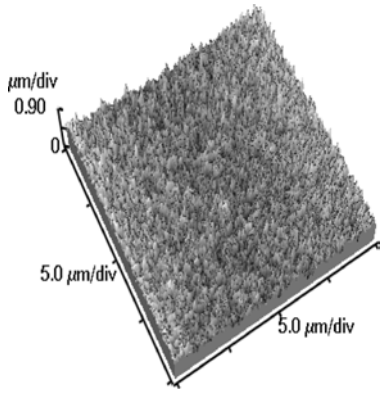

Fig. 9. Atomic force microscope picture of a silicon sample that received a black silicon treatment on its surface.

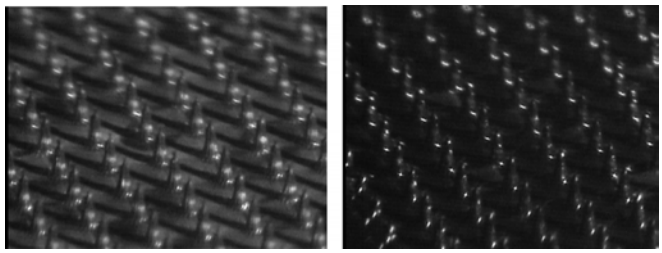

Fig. 10. Field view of a pencil forest before propellant transport (left) and after propellant transport (right), to demonstrate the use of black silicon as wicking material for EMI-BF_4.

that substantially increase the free surface of the substrate, thus augmenting its wettability. The wettability contact angle for several silicon samples, with respect to EMI-BF_4, was measured using a Ramé–Hart contact angle goniometer model 100. The wetting angle of the untreated silicon surface was found equal to 27°, while the contact angle of the silicon sample with the optimized *black silicon* treatment was found to be smaller than 0.5°, causing strong spread enhancement of the EMI-BF_4 liquid on the silicon treated surface.

Fig. 10 shows a series of pictures to illustrate the propellant transport due to surface tension effects for a propellant droplet placed at the center of an emitter array treated with the optimized *black silicon* recipe. In the left-hand side picture of Fig. 10, the emitter array is free of propellant. In the right-hand side picture, a thin liquid film, transported by surface tension

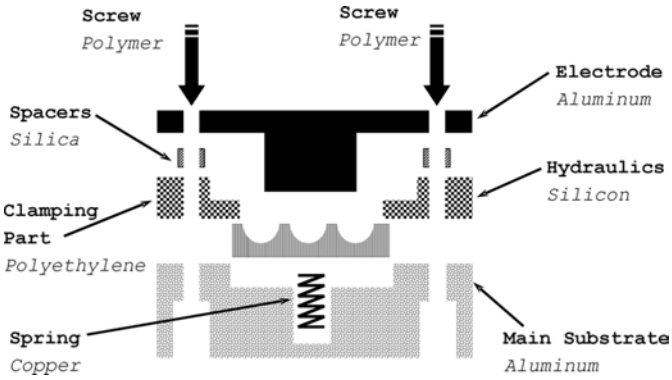

Fig. 11. Schematic of the apparatus used to obtain imprints of the engine fans. The emitter to electrode separation was fixed at 250 μm.

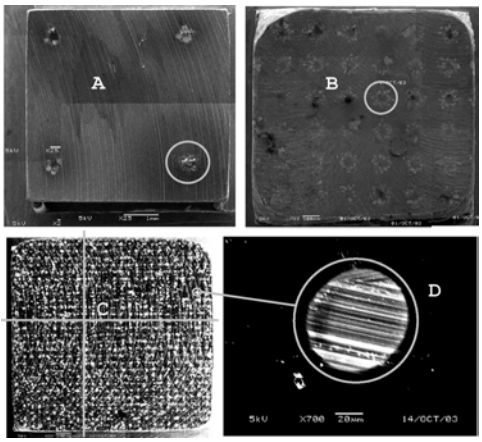

Fig. 12. Collage of SEM pictures to validate the uniformity emission claim. Imprints of the exit stream on collectors using planar electrospray thruster arrays: (A) 2×2 array of 8-tip volcano emitters at 51.3°; (B) 8×8 8-tip volcano emitter array at room temperature. The circles surround selected impact sites; imprints of the exit stream on a collector using a 32×32 pencil emitter planar electrospray thruster array (C), and zoom of the fine imprint of a single emitter (D). The collector area in all cases is 6.8×6.8 mm^2.

effects, covers the emitter array after about a minute since the propellant first made contact with the emitter array surface.

B. Emission Uniformity Tests

After wettability tests were made, the next battery of tests was intended to demonstrate emission uniformity, both from *I–V* characteristics and plume imprints on a collector electrode. Fig. 11 shows an schematic of the apparatus that was used to obtain the *I–V* characteristics and the collector imprints. The emitter-to-collector separation was fixed at 250 μm while the collector voltage was varied between 0 and 3250 V dc. The pressure inside the vacuum chamber was smaller than 10^{-7} torr while tests were in progress.

A key test of device operation is to determine if all electrospray emitters in an array are functioning. The best way to observe this is in real time; however, short of that approach, we chose to monitor the material deposited by the emitters on a collector (collector imprints) after operation. Fig. 12 is a collage of SEMs of collector imprints take after operation of various devices. Fig. 12(a) is an SEM of a 2×2 array of octagonal (8-tip) volcano emitters operating at 51.3 °C while Fig. 12(b) is an SEM of an 8×8 array of octagonal (8-tip) volcano emitters operating at room temperature. In Fig. 12(a) and (b), SEMs taken at higher magnification clearly indicate 8 distinct collector imprint patterns for each emitter, corresponding to the 8-tips of each emitter. This is also an indication that the emission semi-angle is very narrow. Fig. 12(c) is an SEM of collector imprints for a 32×32 array of pencil electrospray emitters. The striations of the background are from the machining of the aluminum collector. Fig. 12(c) shows a two-dimensional array of deposited dots arranged in a square pattern corresponding to the electrospray emitter array. This figure validates the claim that the emitters are emitting uniformly because all 1024 imprints are registered on the collector, and the imprints are alike. Fig. 12(d) is a close-up SEM of the collector imprint shown in Fig. 12(c) The diameter of the dot is about 70 μm.

C. Fan Divergence Measurements

From Fig. 12(a) and (b) it was determined that the volcano emitters emit propellant from each one of the sharp corners at the top surface. An analysis of the distance between the collector imprints and their position relative to the corners of the volcanoes gives us estimates of the emission tilt angle and the divergence semi-angle for the volcano emitters. Fig. 13 shows the relationship between the emitter tip and the collector imprints, illustrating the ion-emission tilt angle and the ion-emission fan divergence semi-angle. The gap between the emitter and the collector is about 250 μm. The distance between the horizontal position of the emitter and the deposits is about 140 μm, while the imprint corona extends up to about 230 μm farther, corresponding to an ion-emission tilt angle of 41.4°. The tilting angle is close to the 45° theoretical value (sharp corner orientation); a reduction of this ideal angle is expected from the electrostatic pulling of the charged fan towards the collector. From the position and width of the collector imprint relative to the emitter tip, and ion-emission fan semi-angle of 14.1° was estimated.

The pencil emitters eject ions vertically; however, the ions fan out due to space charge effects. From the width of collector deposits and the gap between the collector and the emitters, the fan divergence semi-angle is estimated at 9.5°. The divergence semi-angle measurements for both volcanoes and pencils are in agreement with divergence semi-angles reported in the literature, and a reduced order model presented by Lozano [23].

D. I–V Characteristics

Fig. 14 shows the *I–V* characteristics of two emitter arrays with exactly the same emitter type and emitter dimensions, but different number of emitters. The two emitted current/emitter versus voltage characteristics agree, except for a small region near the start-up voltage. This transition region might be due to non-idealities in emission due to the collector not being parallel to the emitter array (variations in the emitter-to-collector distance produce variations in the start-up voltage, as predicted by the reduced-order model). Another possible reason is nonuniformity in the dimensions of the emitters within the array that lead to the existence of a start-up voltage band because all the emitters do not turn-on at the same voltage. On the other hand, the lack of perfect match-up can be related to a shift in the start-up voltage due to the difference in the emitter density between the

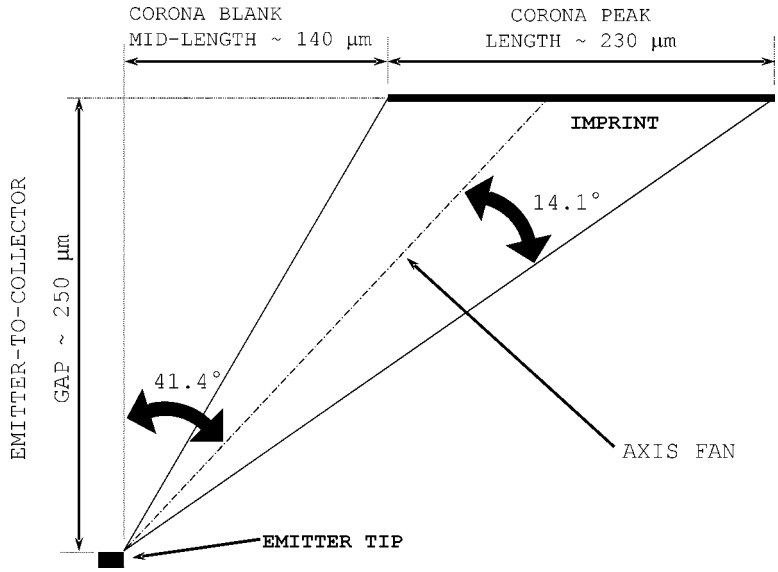

Fig. 13. Schematic to illustrate the fan semi-angle and the fan axis tilting angle, based on the corona peaks for a volcano emitter.

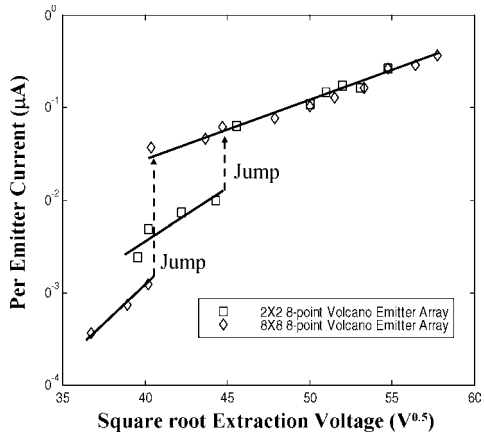

Fig. 14. Current per-emitter versus square root of the extraction voltage for two different arrays with different emitter densities but the same emitter kind and size (one emitter is defined here as one 8-point volcano).

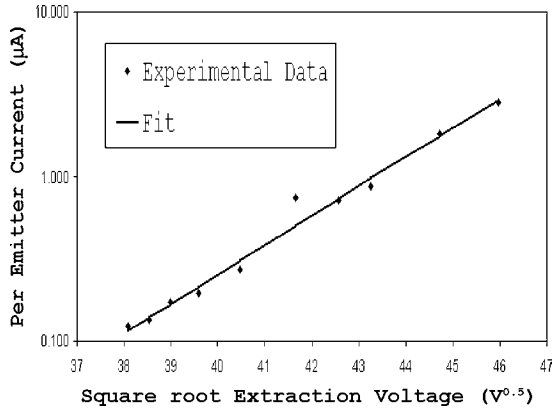

Fig. 15. Current per-emitter versus square root of the extraction voltage for a planar array at a controlled temperature equal to 51.3°C.

two arrays. It is important to point out that the current levels for bias voltages close to the start-up voltage are of the order of nano-amperes, and the signal-to-noise ratio might not be adequate to draw good conclusions. Nonetheless, the emitted currents are of the same order of the currents emitted by tungsten needles using EMI-BF_4 as propellant in a surface driven propellant supply [27].

Finally, a temperature-controlled test was conducted to explore the possibility of substantially increasing the emitted current for a fixed voltage. It has been reported in the literature that the viscosity of EMI-BF_4 substantially decreases, while its electrical conductivity substantially increases, for a rather small temperature change [25]. Fig. 15 shows the *I–V* characterization for an emitter array heated to 51.3 °C, where a current increase of 20 times is obtained. This is much more than the factor of about 3 for changes of viscosity or conductivity over the same temperature range. More recent tests [32] indicate that the temperature effect may not be reversible, but rather in the nature of a *conditioning* of the surface, which persists after the temperature has been returned to its original value. More work is needed to clarify this complex behavior.

In all *I–V* characterizations the experimental data can be described by using a simple exponential fit of the form

$$I = I_o(T) \cdot e^{[V/V_\circ(T)]^n} \tag{8}$$

where I_o, V, and n are fit constants, but, as it will be seen in the following section of this paper, there is uncertainty on the exponent n.

V. Discussion on Field Emission and the *I–V* Characterization

Pending development of a complete model for the emitted ionic current, possibly along the lines of LMIS models [29], only some observations can be made at this point. The more-or-less exponential variation of current with voltage (at a fixed temperature) is reminiscent of the behavior of some limiting ion emission laws. If in (8) we had n equal to 0.5, the Schottky emission model would be obtained; if n is equal to 1, the strong-field limit Pool–Frenkel emission model results, while if n is set

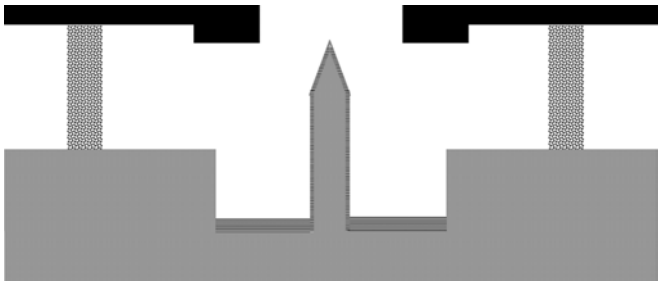

Fig. 16. Schematic of an stratified electrode. The distance between the extractor and the emitter body is maximized at the insulation columns, while the emitter tips are brought as close as possible to the extractor rings to decrease the start-up voltage.

at -1, then the Fowler–Nordheim emission model is obtained [33]. The range of extraction voltages used in the tests appears to be insufficient to provide a precise determination of n. If a Schottky emission model is used, then the data correlation coefficient is found equal to 0.9854, while the adoption of a Pool–Frenkel model gives a correlation of 0.9895. In any of those cases, the implication would appear to be that emission is limited by the surface electric field value, and not by the supply of fluid to the emission site.

If, on the contrary, the current were limited by the rate of fluid supply, a balance of viscous drag versus electrostatic pull (at a fixed geometry) would indicate a quadratic law of the form

$$I \propto \frac{V^2 - V_o^2}{\mu(T)} \tag{9}$$

with V_o being the threshold voltage and $\mu(T)$ de viscosity, dependent on the temperature T. Aside from the different voltage dependence, this model would predict a current variation inverse of that of the viscosity. In tests using EMI-BF_4 with tungsten needles that are surface-patterned using wet chemicals, Lozano reports current increase by a factor of 3 in the same temperature range, which is consistent with the known variation of the fluid viscosity [27]. Our tests, which show factors of the order of 20, would appear inconsistent with this model. Unfortunately, the recent observation of temperature irreversibilities further complicates the issue of temperature dependence, and any viscous effect could be masked by an apparently larger hysteretic effect.

VI. Future Work

In order to take advantage of the clustering potential of this engine concept, a suitable micro-fabricated electrode system must be developed. This way, the engine can operate closer to the space charge limited emission mode, with the corresponding efficient usage of the emitter space available. Regardless of the electrode system implemented, it should satisfy the following criteria:

- implementation of a standoff system to minimize the contact area between the electrodes and the substrate;
- optimization of the emitter-to-extractor distance and insulation gap. One way to implement this optimization would be a stratified extractor, as shown in Fig. 16;
- robust electrode alignment.

It is desirable as well to systematically use the physics of the emission and wicking materials to generate a more reliable engine design model that can predict the *I–V* characteristics. Also, different emitter architectures should be developed to maximize the emitter density; nonetheless, it seems the constraints imposed by field enhancement and fabrication would not allow space charge limited emission [18].

Finally, more research on the elimination/decrease of the electrochemical effects using ac operation is needed to extend the engine lifespan and avoid the use of external neutralization. In this regard, ac operation of an array of 16 8-point volcanoes has been recently demonstrated by Lozano [32], with general features comparable to those earlier observed with Tungsten needles [27], but more detailed work is still pending.

VII. Conclusion

This work reported a hybrid micro-fabricated and macro-fabricated silicon-based planar array of electrospray emitters for thruster applications that uses EMI-BF_4 as propellant. It also demonstrated the feasibility of high clustering, and uniform-steady operation of emitter arrays fed by the same propellant pool. The paper also reported small divergence semi-angle of the emission fan that is in agreement with the literature and a reduced order model, and the possibility to vary the emission currents using temperature. However, the details of the emission mechanism need to be determined. Finally, the experimental current/emitter–voltage characteristics of the planar arrays could be described by a simple exponential fit; however, there is uncertainty in the specific exponent of the voltage dependence.

Acknowledgment

The authors would like to express their gratitude to the staff of MIT's Micro-fabrication Technologies Laboratory (MTL) for their help on the fabrication of the planar array test structures.

References

[1] W. Gilbert, *De Magnete, Magneticisque Corporibus*. London: , 1600.
[2] J. Zeleny, "The electrical discharge from liquid points and a hydrostatic method to measure electric intensity at their surface," *Phys. Rev.*, vol. 3, pp. 69–91, 1914.
[3] G. I. Taylor, "Disintegration of water drops in an electric field," *Proc. R. Soc. London A*, vol. 280, no. 1382, pp. 383–397, 1964.
[4] J. Perel, "Research on a charged particle bipolar thrustor," in *Proc. AIAA Electric Propulsion Plasmadynamics Conf.*, Colorado Springs, CO, 1967, 67A728.
[5] ——, "Analytical study of colloid annular thrusters," in *Proc. AIAA 8th Electric Propulsion Conf.*, Stanford, CA, 1970, 70A1113.
[6] ——, "Experimental study of colloid annular thrusters," in *Proc. AIAA 8th Electric Propulsion Conf.*, Stanford, CA, 1970, 70A1112.
[7] ——, "Colloidal annular array thruster development," in *Proc. AIAA 10th Electric Propulsion Conf.*, Lake Tahoe, Nevada, 1973, 73A1077.
[8] ——, Mechanisms of Emitter Surface Damage during Electrohydrodynamic Colloid Particle Generation and Acceleration AFOSR Contract F44620-75-C-0056, AFOSR TR 78 – 1026, 1978.
[9] A. Bailey, "Temperature effects and capillarity in an electrostatic thruster," in *Proc. AIAA 11th Electric Propulsion Conf.*, New Orleans, LA, 1975, 75A434.
[10] J. Mueller, "Thruster Options for Micro-Spacecraft: A Review and Evaluation of Existing Hardware and Emerging Technologies," in *Proc. 33rd AIAA/ASME/SAE/ASEE Joint Propulsion Conf. and Exhibit*, Seattle, WA, 1997, AIAA 1997-3058.
[11] J. B. Fenn, "Colloid ionization for mass spectrometry of large biomolecules," *Science*, vol. 246, pp. 64–71, 1989.
[12] V. Hruby, "Micro newton colloid thruster system development," in *Proc. 27th Int. Electric Propulsion Conf.*, Pasadena, CA, 2001, IEPC-01-281.
[13] M. Paine, "Design Study for Micro-Fabricated Colloidal Thrust," M.S. thesis, Dept. Aeronaut. Astronaut., Massachusetts Institute of Technology, Cambridge, 1999.

[14] ——, "A micro-fabricated colloid thruster array," in *Proc. 37th AIAA/ASME/SAE/ ASEE Joint Propulsion Conf. and Exhibit*, Salt Lake City, UT, 2001, AIAA 2001-3329.
[15] J. Xiong, "The design, fabrication, and test of a MEMS-based micro-colloid thruster," *Proc. SPIE*, vol. 4928-24, 2002.
[16] ——, "A colloid microthruster system," *Microelectron. Eng.*, vol. 61–62, pp. 1031–1037, 2002.
[17] L. F. Velásquez, "A Micro-Fabricated Colloid Thruster Array," M.S. thesis, Dept. Aeronaut. Astronaut., Massachusetts Institute of Technology, Cambridge, 2001.
[18] ——, "The Design, Fabrication and Testing of Micro-Fabricated Linear and Planar Colloid Thruster Arrays," Ph.D. dissertation, Dept. Aeronaut. Astronaut., Massachusetts Institute of Technology, Cambridge, 2004.
[19] L. F. Velásquez *et al.*, "Advances in micro–fabricated droplet emission mode 1D colloid thruster array," in *Proc. Space Propulsion 2004*, Sardinia, Jul. 2004.
[20] M. Gamero-Castaño, "Electric measurements of charged sprays emitted by cone-Jets," *J. Fluid Mech.*, vol. 459, pp. 245–276, 2002.
[21] J. Fuller *et al.*, "Structure of 1-ethyl-3-methylimidazolium hexafluorophosphate: model for room temperature molten salts," *J. Chem. Soc., Chem. Commun.*, vol. 3, pp. 299–300, 1994.
[22] J. de la Mora, "Source of heavy molecular ions based on taylor cones of ionic liquids operating in the pure ion evaporation regime," *J. Appl. Phys.*, vol. 94, no. 5, pp. 3599–3605, 2003.
[23] P. Lozano, "Studies on the Ion-Droplet Mixed Regime in Colloid Thrusters," Ph.D. dissertation, Dept. Aeronaut. Astronaut., Massachusetts institute of Technology, Cambridge, 2003.
[24] Y. Chiu, "Mass spectrometric analysis of ion emission for selected colloid thruster fuels," in *Proc. 39th AIAA/ASME/SAE/ASEE Joint Propulsion Conf. Exhibit*, Huntsville, AL, 2003.
[25] J. Fuller, "The room temperature ionic liquid 1-ethyl3-methylimidazolium tetrafluoroborate: Electrochemical couples and physical properties," *J. Electrochem. Soc.*, vol. 144, pp. 3881–2886, 1997.
[26] P. Lozano and M. Martinez-Sanchez, "Efficiency estimation of EMI-BF_4 ionic liquid electrospray thrusters," in *Proc. 41th AIAA/ASME/SAE/ASEE Joint Propulsion Conf. Exhibit*, Tucson, AL, 2005.
[27] ——, "Ionic liquid ion sources: Characterization of externally wetted emitters," *J. Colloid Interface Sci.* , vol. 282, no. 2, pp. 415–421, 2005.
[28] ——, "Ionic liquid ion sources: Suppression of electrochemical reactions using voltage alternation," *J. Colloid Interface Sci.*, vol. 280, no. 1, pp. 149–154, 2004.
[29] G. L. Mair*, Link Focused Ion Beams from Liquid Metal Ion Sources*. New York: Wiley, 1991.
[30] S. P. Thompson and P. D. Prewett, "The dynamics of liquid metal ion sources," *J. Phys. D: Appl. Phys.*, vol. 17, pp. 2305–2321, 1984.
[31] H. Jansen, "The black silicon method: A universal method for determining the parametric setting of a fluorine-based reactive ion etcher in deep silicon trench etching with profile control," *J. Micromech. Microeng.*, vol. V5, no. 2, pp. 115–120, Jun. 1995.
[32] P. Lozano, Private Communication.
[33] R. Gomer*, Field Emission and Field Ionization*. New York: American Institute of Physics, 1993.

Luis Fernando Velásquez-García received the Mechanical Engineer degree (*magna cum laude*) and the Civil Engineer degree (*magna cum laude*) from Los Andes University, Bogotá, Colombia, in 1998 and 1999, respectively, and the M.S. degree in aeronautics and astronautics and the Ph.D. degree in space propulsion from the Massachusetts Institute of Technology (MIT), Cambridge, in 2001 and 2004, respectively.

After completing his studies, he became a Postdoctoral Associate (2004) affiliated with the MIT's Microsystems Technology Laboratories (MTL), and the Gas Turbine Laboratory (GTL). Since 2005, he has held an appointment as Research Scientist, affiliated with the same laboratories at MIT. His research focuses on micro– and nano–fabrication technologies applied to propulsion, structures, and power systems. He has conducted research in micro- and nano-technology applied to electrospray arrays, mass spectrometry, field emission, mass/charge sensors, 3-D packaging, electron impact ionization, field ionization, plasma–enhanced chemical vapor deposition, carbon nano-tube–based devices, turbomachinery, and chemical lasers.

Akintunde Ibitayo Akinwande (M'00) received the B.Sc. degree in electrical and electronic engineering from the University of Ife, Ife, Nigeria, in 1978, and the M.S. and Ph.D. degrees in electrical engineering from Stanford University, Stanford, CA, in 1981 and 1986, respectively.

He joined the Honeywell Technology Center, Bloomington, MN, in 1986, where he initially conducted research on GaAs complementary FET technology for very-high-speed signal processing. He later joined the Si Microstructures Group, where he conducted research on pressure sensors, accelerometers, thin-film field emission, and display devices. He joined the Microsystems Technologies Laboratories, Massachusetts Institute of Technology (MIT), Cambridge, in 1995, where his research focuses on device and micro-fabrication technologies with particular emphasis on smart displays, large-area electronics, field emission and field ionization devices, and electric propulsion. He is currently a Professor in MIT's Electrical Engineering and Computer Science Department. He holds four patents in MEMS and display technologies and has authored more than 50 journal publications.

Prof. Akinwande is a recipient of the 1996 National Science Foundation Career Award. He has served on a number of technical program committees for various conferences, including the Device Research Conference, the International Electron Devices Meeting, the International Solid-State Circuits Conference, the International Display Research Conference, and the International Vacuum Microelectronics Conference.

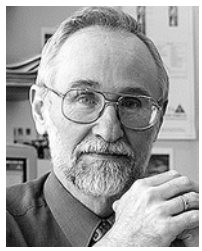

Manuel Martínez-Sánchez received the Aeronautical Engineer's degree from the Polytechnic University of Madrid, Madrid, Spain, in 1967, and the Ph.D. degree from the Massachusetts Institute of Technology (MIT), Cambridge, in 1973.

His professional career has been entirely as a teacher at MIT, where he is currently a Professor of Aeronautics and Astronautics. His research and teaching are concentrated on space propulsion, after having in the past looked into MHD power generation and other energy-related topics. He is currently director of the MIT Space Propulsion Laboratory, where theoretical and experimental research is being conducted on plasma thrusters, thruster plumes, and micro-propulsion using electrospray phenomena. He has authored about 30 journal papers and 120 conference papers.

Prof. Martínez-Sánchez is a Corresponding Member of the Spanish Academy of Engineering.